Corrugation Instabilities Across Shock Fronts in Magnetohydrodynamical Astrophysical Systems

by
Austin Charles Mullins

A THESIS

submitted to

Oregon State University

Honors College

in partial fulfillment of
the requirements for the
degree of

Honors Baccalaureate of Science in Physics
(Honors Scholar)

Presented June 3, 2020
Commencement June 2020

AN ABSTRACT OF THE THESIS OF

Austin Charles Mullins for the degree of Honors Baccalaureate of Science in Physics presented June 3, 2020. Title: Corrugation Instabilities Across Shock Fronts in Magnetohydrodynamical Astrophysical Systems.

Abstract approved:_____

Kathryn Hadley

Slow magnetosonic shock fronts are unstable to changes made to their shape, a phenomenon known as corrugation instability. The computational models studied considers a system where plasma travels across a shock front. Using the code Linogen, the corrugation instability of a shock front can be theoretically modeled. The results show how corrugation instability changes with an increase in Alfvenic Mach number and sonic Mach number over a series of angles and transverse wave vector components. This series of angles describe the angle of entry at which the fluid penetrates the shock front from the normal of the shock front. Entry angles ranged from $\beta=15^{\circ}$ to $\beta=45^{\circ}$. It was found that for smaller angles, the shock front became more unstable quicker as the Alfven Mach number increased whereas for larger angles the shock front grew more unstable slower as the Alfven Mach number increased. It was also found that the shock front became more unstable quicker as the sonic Mach number increased for smaller angles. Small Alfven Mach numbers described strong magnetic fields. Small sonic Mach numbers describe slow moving fluid. Corrugation instabilities become of interest when studying astrophysical systems such as T-Tauri stars and neutron stars.

Key Words: Alfven mode, corrugation instability, entropy mode, Linogen, magnetohydrodynamics, magnetosonic modes, shock front, T-Tauri star.

Corresponding e-mail address: austincmullins@hotmail.com

Corrugation Instabilities Across Shock Fronts in Magnetohydrodynamical Astrophysical Systems

by
Austin Charles Mullins

A THESIS

submitted to

Oregon State University

Honors College

in partial fulfillment of
the requirements for the
degree of

Honors Baccalaureate of Science in Physics
(Honors Scholar)

Presented June 3, 2020
Commencement June 2020

Honors Baccalaureate Science in Physics project of Austin Charles Mullins presented on June 3, 2020.

APPROVED:

_____

Kathryn Hadley, Mentor, representing Department of Physics

_____

Henri Jansen, Committee Member, representing Department of Physics

_____

Randall Milstein, Committee Member, representing Department of Physics and Department of Earth, Ocean, and Atmospheric Sciences

_____

Toni Doolen, Dean, Oregon State University Honors College

I understand that my project will become part of the permanent collection of Oregon State University, Honors College. My signature below authorizes release of my project to any reader upon request.

_____

Austin Charles Mullins, Author

List of Figures

Contents

Chapter 1

Introduction

1.1 Motivation and Objective

This project focuses on the analysis of the ideal magnetohydrodynamic (MHD) continuity equations, the MHD waves that propagate away from a shock front, and the unstable growth of perturbations made to the shape of a shock front. The latter is commonly referred to as corrugation instability. A shock front is created when fluid moving at supersonic speed collides with fluid moving at subsonic speed. The wave modes studied include Alfven modes, magnetosonic modes (slow and fast), and the entropy mode. These waves are launched upstream and downstream as a result of fluid striking a shock front. Code written in MATLAB is used to find how the shape of the shock front changes as fluid passes through it at different Mach numbers. The overall goal outlined in this paper is to compute the eigenvalues of the MHD system and model growth rate of the corrugation instability. Two specific cases are studied, the Lessen and Deshpande case which considers the transverse z-component of the wave vector, $\vec{k}$, to be zero and the general case which considers the transverse z-component of the wave vector, $\vec{k}$, to be nonzero. The corrugation instabilities studied consider pre-shock and post-shock conditions that allow for the modeling of the unstable growth of perturbations to a shock front to be visualized.

1.2 Relevant Systems

This project is interesting because the current understanding of astrophysical systems such as T-Tauri stars and neutron stars involves plasma following onto the surface of the central star. Considering the flow of plasma, plasmas moving at different velocities is probable making such astrophysical systems accustom to the development of shock fronts that undergo perturbations that change their shape. Understanding shock fronts and their evolution is a useful tool in further understanding the nature of T-Tauri stars and neutron stars.

1.3 Hydrodynamical Shocks

Before understanding the MHD shocks in astrophysical systems discussed throughout this paper, it's important to understand hydrodynamical shocks that are seen here on Earth first. One of the best examples used to describe a hydrodynamical shock is the white plume that forms around a jet plane when a jet plane travels at a velocity exceeding that of the speed of sound. The speed of sound is described using Mach numbers (i.e. Mach 1 is equal to the speed of sound). Mach numbers above 1 define velocities faster than the speed of sound and Mach numbers below 1 define velocities slower than the speed of sound. When a jet plane reaches a velocity above Mach 1, a white plume forms around the jet plane. This white plume is called a vapour cone or shock front. This plume is a result of a process known as Prandtl-Meyer Expansion Fan. The Prandtl-Meyer Expansion Fan process leads to an infinite number of Mach waves or high velocity pressure waves to form and spread out. The localized increase in velocity causes pressure in the air to decrease which in turn drops the surrounding air temperature. If there is enough moisture in the air, the temperature of the air falls below the dew point causing condensation to form. This condensation makes up what looks to be a white plume or shock front around the jet plane. With this information, we can now introduce a system that is influenced by the presence of a magnetic field and study MHD shocks.

1.4 MHD in Astrophysical Sytems

MHD is the study of the behavior of electrically conducting fluids. In the astrophysical case, this fluid is plasma. Magnetic fields can induce currents in conducting fluid which ultimately polarizes the fluid changing the magnetic field of the system. Plasma, in the case of astrophysical systems, involves conducting gas that moves at supersonic and subsonic speeds. In the research outline in this paper, we are concerned with four main properties of the fluid: plasma velocity, plasma current density, plasma mass density, and plasma pressure. The ideal MHD equations use these properties to further examine the effects of MHD systems. MHD waves can be studied across the fluid that flows onto the surface of T-Tauri stars and neutron stars. Shock fronts can form and evolve as the fluid flows onto the surface of the central star of such astrophysical systems. In a T-Tauri star system, the inner star is made up of hot gas and plasma. This star creates its own magnetic field lines through it spinning on its axis. Fluid on the inner edge of the accretion disk that surrounds the star can fall out of the star's orbit and travel along the magnetic field lines of the star and onto the star's surface. This happens as the result of the fluid on the inner edge of the accretion disk having a high viscosity rendering it too slow to remain in orbit around the star. When the fluid crashes onto the surface of the central star, a shock front is formed. Fluid entering the shock front can either be parallel to the shock front's normal or at some angle β.

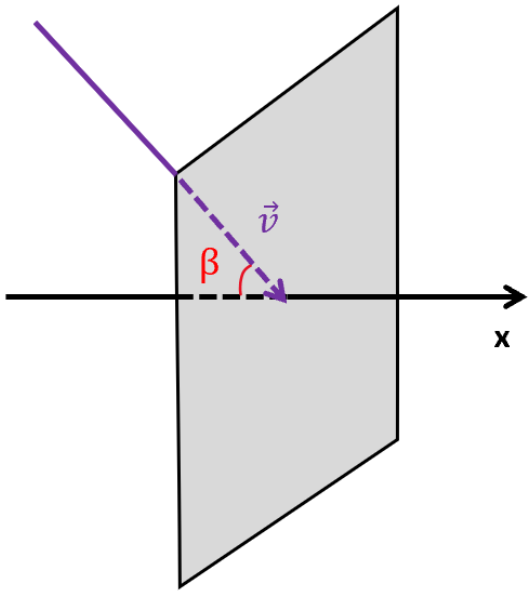

Figure 1.1: Entry of fluid into a shock front nonparallel to the normal of the shock front.

Figure 1.1 visualizes a how a fluid enters a shock front. Shock fronts also have the ability to change the direction of a fluid that passes through it. The focus of this work is to observe how the magnetic field and fluid velocity can evolve the shock front given the properties of the MHD waves that propagate away from the shock front as a result of the entering fluid striking the shock front. For $\beta = 0$, the initial magnetic field of the entering fluid is parallel to the normal of the shock front [3]. In slow shock systems, this condition describes a slow parallel shock. When $\beta \neq 0$, the initial magnetic field of the entering fluid is oblique to the normal of shock. This condition describes a slow oblique shock in slow shock systems. McKenzie and Westphal studied the oblique shock case for fast shocks in [4].

Chapter 2

Theory

2.1 Ideal MHD Equations

A set of five equations governs MHD systems. These equations are derived from fluid dynamics and Maxwell's equations. These equations connect the mass density of the plasma ρ, the velocity of the plasma $\mathbf{v}$, the current density of the plasma $\mathbf{J}$, the gas press P, the total magnetic field strength B, and the adiabatic index for a monatomic ideal gas $\gamma = \frac{5}{3}$ [9]. For MHD equations to properly describe the system, the divergence of the magnetic field must be equal to zero. These equations can be combined and solved to produce the MHD wave equations that are used to describe the wave behavior and shock fronts created by the supersonic plasma colliding with subsonic plasma.

$$\partial t\rho + \nabla \cdot (\rho \mathbf{v}) = 0 \tag{2.1}$$

$$\rho(\partial t + v \cdot \nabla)\mathbf{v} + \nabla P + \rho \nabla \phi_g - \frac{\mathbf{J} \times \mathbf{B}}{c} = 0 \tag{2.2}$$

$$\partial t\mathbf{B} - \nabla \times (\mathbf{v} \times \mathbf{B}) = 0 \tag{2.3}$$

$$\nabla \cdot \mathbf{B} = 0 \tag{2.4}$$

$$\partial tE + \nabla \cdot [(\frac{\rho v^2}{2} + \frac{\gamma P}{\gamma - 1})\mathbf{v} - (\mathbf{v} \times \mathbf{B}) \times \mathbf{B}] = 0 \tag{2.5}$$

Equation 2.1 describes mass continuity, equation 2.2 describes momentum conservation, equation 2.3 describes magnetic induction derived from Maxwell's equations, equation 2.4 describes magnetic divergence, one of Maxwell's equations, and equation 2.5 describes energy conservation.

These equations can be linearized into the following form:

$$\rho, \mathbf{v}, \mathbf{B} \rightarrow \mathbf{B} = \mathbf{B}_0 + \mathbf{B}_1 e^{i(\vec{k}\cdot\mathbf{r}-\omega t)} \tag{2.6}$$

2.2 Ideal MHD Shock Jump Conditions

The ideal MHD shock jump conditions take the linearized pre-shock ideal MHD equations and the linearized post-shock ideal MHD equations and stitch them together. The ideal shock jump conditions use the same variables as the ideal MHD equations but consider perpendicular and parallel quantities to the shock front normal. The plasma velocity term v as defined in the ideal MHD equations is replaced with U in this set of conditions and enthalpy is added using the symbol H.

$$[\rho U_\perp]_1^2 = 0 \tag{2.7}$$

$$[P + \rho U_\perp^2 + \frac{(B_\parallel^2 - B_\perp^2)^2}{4\pi}]_1^2 = 0 \tag{2.8}$$

$$[U_\perp^2 \mathbf{U}_\parallel - \frac{B_\perp \mathbf{B}_\parallel}{4\pi}]_1^2 = 0 \tag{2.9}$$

$$[U_\perp \mathbf{B}_\parallel - \mathbf{U}_\parallel B_\perp]_1^2 = 0 \tag{2.10}$$

$$[B_\perp]_1^2 = 0 \tag{2.11}$$

$$[U_\perp(\frac{\rho}{2}(U_\perp^2 + U_\parallel^2) + \rho H) + \frac{1}{4\pi}(U_\perp B_\parallel^2 - (\mathbf{U}_\parallel \cdot \mathbf{B}_\parallel)B_\parallel)]_1^2 = 0 \tag{2.12}$$

Equation 2.7 is conservation of normal mass flux, equation 2.8 is conservation of normal momentum, equation 2.9 is conservation of tangential momentum, equation 2.10 is conservation of the tangential **E** field in terms of the magnetic field, equation 2.11 is the divergence of the magnetic field, and equation 2.12 is conservation of energy. The notation used to define the conditions takes on the following form:

$$\rho_1 U_{\perp 1} = \rho_2 U_{\perp 2} \rightarrow [\rho U_\perp]_1^2 = 0 \tag{2.13}$$

Here the subscript 1 defines the pre-shock conditions and the subscript 2 defines the post-shock conditions. The symbol $\perp$ defines components perpendicular to the shock front's normal and the symbol $\parallel$ defines components parallel to the shock front's normal.

2.2.1 MHD Wave Modes

There are three types of wave modes that make up an MHD system. These modes include the Alfven mode, magnetosonic modes which are similar to sound waves, and the entropy mode. These waves propagate through a fluid as the result of fluid striking a shock front. The Alfven mode propagates both upstream and downstream from the shock front. Magnetosonic modes can be broken up into two different types: fast and slow. Both types, like Alfven modes, propagate upstream and downstream from the shock front. The entropy mode is a wave with zero velocity with respect to the fluid. The entropy mode can therefore be seen as a mode that simply travels at the velocity of the fluid and only travels downstream from the shock front. These three modes make up a total of seven different waves that each have their own wave properties.

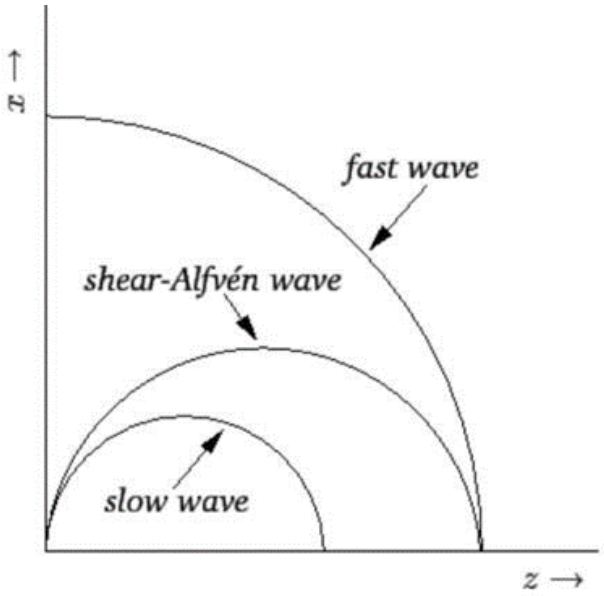

Figure 2.1: Speed of the two magnetosonic waves vs the Alfven wave [2].

Figure 2.1 visualizes the phase velocities of the two magnetosonic modes and the Alfven mode. The entropy mode is not included since it travels at zero velocity with respect to the fluid. The other two modes travel with some nonzero velocity with respect to the fluid unlike the entropy mode.

2.2.2 Alfven Mode

Disturbance of the equilibrium of a magnetic field causes transverse vibrations in the magnetic field lines. As a result of this disturbance, Alfven waves are formed. An Alfven wave in MHD is a transverse wave that propagates parallel to the magnetic field [10]. Alfven waves have a constant group velocity. The wave velocity can be determined by the ratio of the initial magnetic field strength of a fluid striking a shock front (B_0) and the density of the fluid (ρ) multiplied by a factor of 4π.

$$v_A = \frac{B_0}{\sqrt{4\pi\rho}} \tag{2.14}$$

2.2.3 Magnetosonic Modes

Longitudinal oscillations can also occur in magnetic field lines, these are sound waves or compression waves where particles are free to move. These types of waves are known as magnetosonic waves. Two types of magnetosonic waves are present in MHD systems: fast magnetosonic waves and slow magnetosonic waves. Figure 2.1 visualizes how the phase velocities of the two magnetosonic modes compare to the Alfven mode. The velocity of the two magentosonic modes is described using the following relationship:

$$v_{\pm} = (\frac{w}{k})^2 = \frac{1}{2}[({v_A}^2 + {c_s}^2) \pm \sqrt{({v_A}^2 + {c_s}^2) - 4{v_A}^2{c_s}^2 cos^2\psi}] \tag{2.15}$$

In equation 2.15, the fast magnetosonic wave is characterized by $+$ and the slow magentosonic wave is characterized by $-$. w describes the angular frequency of the wave, $\vec{k}$ is the wave vector, v_A is the Alfven speed described by equation 2.14, c_s is the speed of sound, and ψ is the angle between B_0 and the wave vector $\vec{k}$.

2.2.4 Entropy Mode

The entropy mode as defined earlier moves with zero velocity with respect to the fluid. Therefore, the velocity of the entropy wave is equal to zero compared to the velocity of the other two MHD wave modes. This strike propagates downstream only with the fluid unlike the magentosonic waves and Alfven wave. However, this wave still plays a role in the creation of perturbations made to the shape of a shock front.

2.3 MHD Shocks

A shock is a discontinuity separating two different regimes in an otherwise continuous medium [8]. When the velocity of a fluid exceeds the velocity of signal propagation, a shock is formed. A better description of this concept happens in the earlier described hydrodynamical example and astrophysical MHD systems. A shock is formed by the plasma flowing onto the surface of the central star of a T-Tauri star system or a neutron star system when the fluid flowing onto the surface of the central star is moving at supersonic speed and collides with fluid on the surface of the star moving at subsonic speed. Since stars created their own magnetic field, sometimes fluid orbiting the star falls out of orbit and follows the magnetic field lines created by the star. This describes how fluid moves onto the surface of a central star. The region where the two fluids collide forms a infinitely thin plane that can be referred to as a shock front. This work seeks to study how this shock front changes shape.

2.3.1 Fast and Slow Shocks

Fast and slow MHD shocks are the two types of shocks that can form when supersonic fluid crashes into subsonic fluid. In the case of a fast shock front, the magnetic field is refracted away from the shock normal and the total magnetic field strength increases [5]. In the case of a slow shock front, the magnetic field is refracted towards the shock normal and the total magnetic field strength decreases.

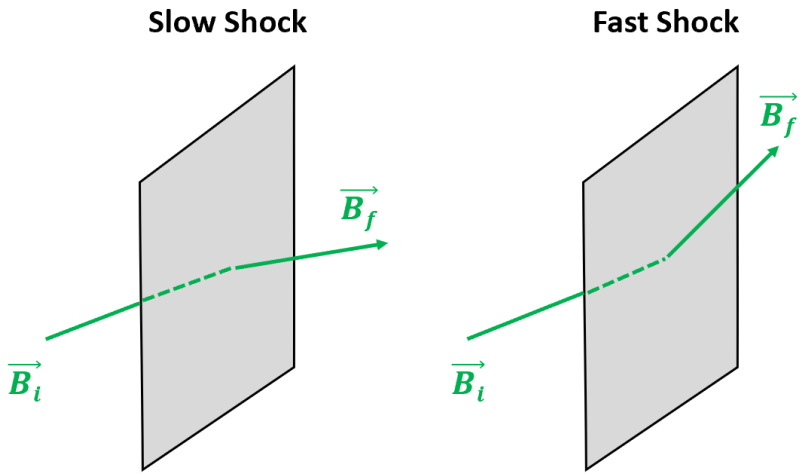

Figure 2.2: The effect of the magnetic field across fast and slow shock fronts.

Figure 2.2 shows how the two shock fronts can bend a magnetic field. This bending of the magnetic field alters the orientation of the wave modes propagating away from the shock front. Understanding how the shock front changes the orientation of a magnetic field provides insight on the orientation of wave modes propagating upstream and downstream from the shock. The results discussed in Chapter 4 of this paper models slow shocks.

Gardner and Kruskal studied special cases and found that fast shocks are stable [1]. Though special cases were only investigated, it is believed that generally fast shocks are stable. Lessen and Deshpande investigated the stability of slow shocks where the sonic Mach number $Ms = \frac{v_0}{c_s}$ was fixed and Alfven Mach numbers between $0.22 < M_a < 1$ were varied using numerical techniques and found that slow shocks were unstable[7]. Here v_0 is defined as the shock speed and c_s is defined as the sound speed in a pre-shock gas. The Alfven Mach number is defined as the following:

$$M_a = \frac{v_0}{v_A} \tag{2.16}$$

In equation 2.16, v_A is defined by equation 2.14 as the Alfven speed in a pre-shock gas. Therefore, we can

relate the initial magnetic field of fluid entering a shock to the Alfven Mach number. The Alfven Mach number is inversely proportional to the initial magnetic field of the entering fluid so lower Alfven Mach numbers define fluids with stronger initial magnetic fields.

$$M_a = \frac{v_0\sqrt{4\pi\rho}}{B_0} \tag{2.17}$$

2.3.2 Corrugation Instability

Corrugation instability describes how a shock front wrinkles and folds. This warping of a shock front creates "fingers" or instabilities that changes the shape of a shock front. These instabilities can cause a shock front to warp in a way that can cause parts of a shock to "break off" like the solar coronas on the sun.

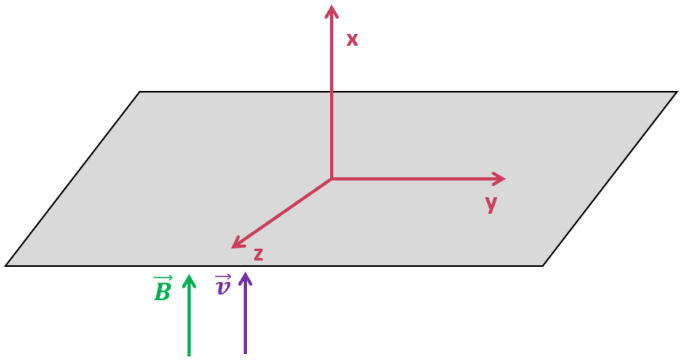

Figure 2.3: Unperturbed shock front.

Figure 2.3 visualizes an unperturbed shock front with fluid propagation along the x-axis. This case describes a parallel shock where the magnetic field is parallel to the shock normal. The shock front is in equilibrium and where since there are no wrinkles or folds to its shape. This shock front would be considered "stable" as this moment in time where the shock front is a flat plane. When a shock front is at equilibrium, there are no perturbations that change the shape of the shock front. As time is evolved and fluid flows through a shock front, the shock front begins to show signs of perturbations to its shape through the wrinkling of the once perfectly planar shock front. Here we begin to consider corrugation instability.

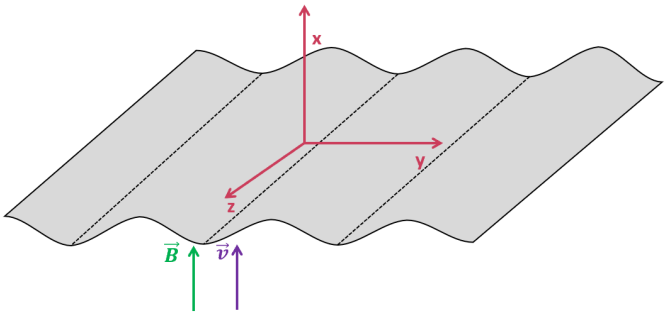

Figure 2.4: Perturbed shock front.

Figure 2.4 visualizes a perturbed shock front with fluid propagation along the x-axis. This case still describes a parallel shock where the magnetic field is parallel to the shock normal similar to figure 2.3. The wrinkling of the once planar shock front animates the effects of the corrugation instability. The unstable growth of perturbations to the system causes the shock front to warp in shape. To further understand how the shape of a shock front is warped by the entering fluid, consider the classical hydrodynamical case absent of a magnetic field where the shock front is shaped sinusoidally. When entering fluid hits a perturbed shock front perpendicular to a shock front's normal, the exit fluid tends to refract towards the troughs of the shock front. Figure 2.5 seeks to visualize this concept.

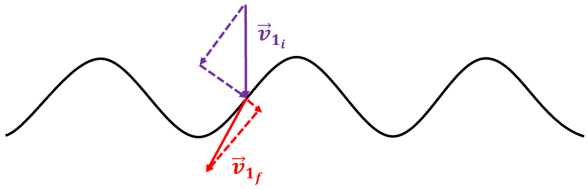

Figure 2.5: Fluid entering a hydrodynamical shock front.

Considering that the fluid is flowing through all points along the shock front and not just one singular point, the refraction of the exit fluid towards the troughs causes the density of the pressure in the trough regions to increase. As the pressure increases in the troughs across the shock front, the troughs will begin to be "pushed up". While this is happening, the entering fluid creates pressure regions along the peaks of the shock front causing these regions to be "pushed down".

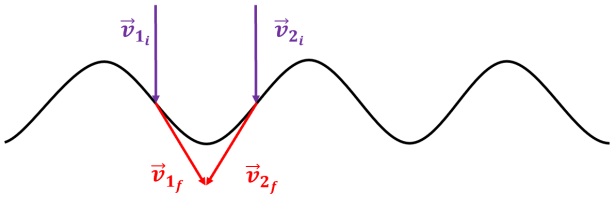

Figure 2.6: Effects of fluid entering a shock front in a hydrodynamical system.

Combing the two effects that causes a change to the shape of the regions of the shock front, the shock front begins to become stable as the amplitude of the peaks and the troughs across the shock front begin to decrease causing the sinusoidal shape of the shock front to flatten out and become planar. Therefore, the shock has reached equilibrium and become stable. The dynamics of this system change when a magnetic field is added to the system via the entering fluid. The introduction of a magnetic field changes the system from one that hydrodynamical to one that is magnetohydrodyanmical.

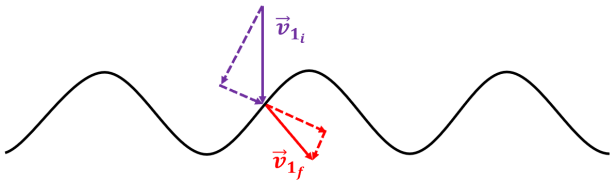

Figure 2.7: Fluid entering a magnetohydrodynamical shock front.

In the MHD case, fluid entering perpendicular to a perturb shock front's normal is refracted towards the peaks of the shape of the shock front. The exiting fluid increases pressure underneath the peaks causing the peaks to increase in amplitude. The pressure caused by the entering fluid causes the troughs to also increase in amplitude. The growth of the wrinkles or the amplitude of the peaks and troughs paints a picture of the corrugation instability of an MHD shock front.

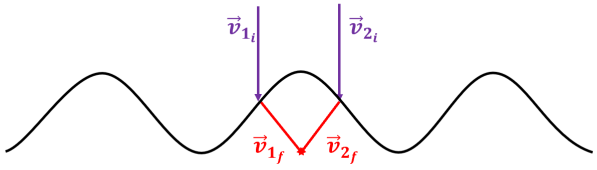

Figure 2.8: Effects of fluid entering a shock front in a magnetohydrodynamical system.

Putting all of this together, visualizing the growth of the instability of the perturbations made to the shape of an MHD shock front is the overall goal that this paper aims to present.

Chapter 3

Modeling Techniques

3.1 Lingoen in MATLAB

The code that models the evolution of the corrugation instability is written in MATLAB. This code will be referred to as Linogen throughout the rest of this paper. Linogen was previous written by a colleague of Dr. Hadley when Dr. Hadley was still a PhD. student at the University of Oregon.

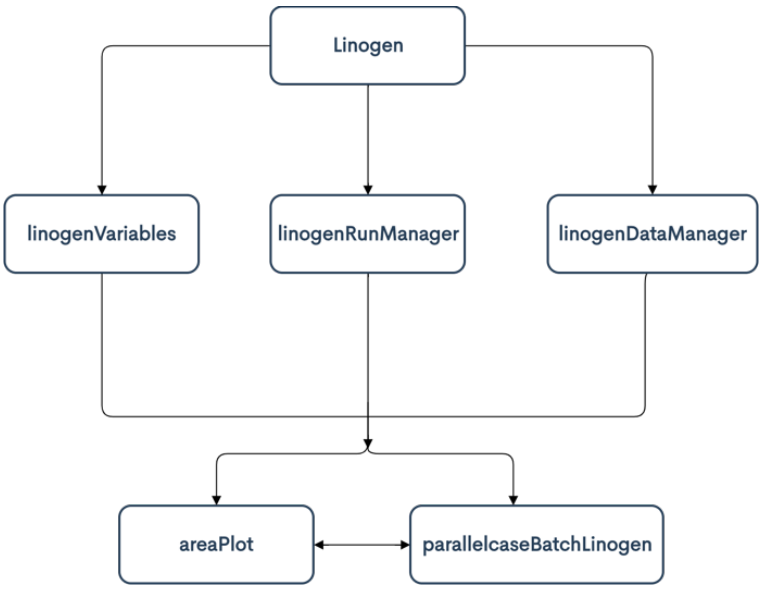

Figure 3.1: A map of the structure of Linogen.

Figure 3.1 is a graphic that describes the structure of Linogen. linogenVariables, linogenRunManager, and linogenDataManager are the three backbone components of the code that house much of the functions and definitions that allow the code to run. Within subroutines is housed the stitched together pre and post shock ideal MHD equations. parallelcaseBatchLinogen pulls from these subroutines and allows for the fluid

Mach numbers to be changed, the angle at which the fluid enters the shock front, and value transverse z-components of the wave vector, $\vec{k}$. Running parallelcaseBatchLinogen results in a block of data that can then be compiled into two different plots. areaPlot is used to determine ω values that are solutions to the evolved system using the MHD equations.

In parallelcaseBatchLinogen, there are two run types: point search and area search. The area search run type solves for the angular frequency, ω, of the wave modes. This angular frequency has both a real and imaginary component. The area search run type is the first thing to run when creating the evolution of the corrugation instability models as the angular frequencies at different inputted fluid entrance angles are used in the point search run type. Once an ω is found for a given angle, the value of ω is inputted into parallelcaseBatchLinogen and the run type is changed from area search to point search. parallelcaseBatchLinogen is then run at a low resolution multiple times to develop an model of the evolution of the corrugation instability at a given angle.

Before running a point search to plot the evolution of the corrugation instability, an ω value must be found at the given angle of interest. This is done using the area search run type. The area search creates a plot that finds ω values that can be used to solve the MHD equations and plot the growth of the perturbations across the shock front. The solution region in area search has two solutions that solve the MHD equations: the trivial solution ($\omega = 0 + 0i$) and a solution you must search for within the plot produced by the area search.

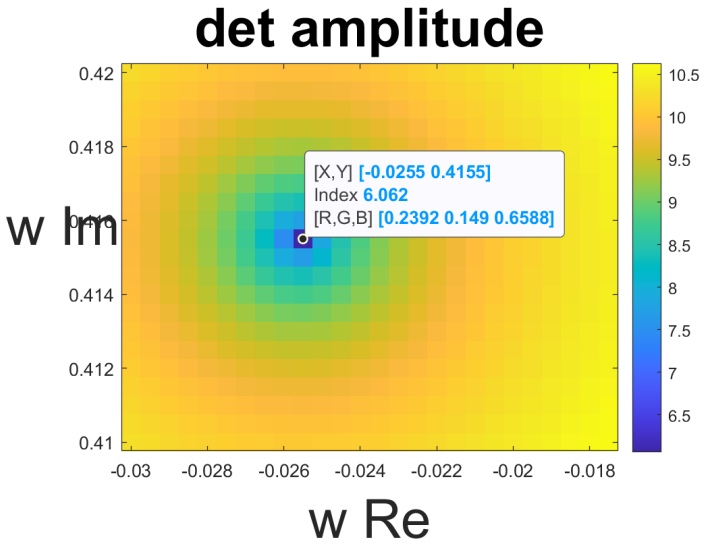

Figure 3.2: Omega value found for a Lessen and Deshpande case model at an input angle of $\beta = 15°$.

Figure 3.2 visualizes the found nontrivial ω value for an area search done at a fluid entry angle of $\beta = 15°$.

The solution is defined by the purple region in the plot. This solution is usually not visible in the first area search run. Location parameters can be changed to make the ω value more visible. MATLAB has a data tips function that pinpoints the solution and reads off the real and imaginary components that make up the solution found in a given the area search plot. This is visualized in figure 3.2.

Low resolution models are run first because they take less time. When attempting to plot the growth of the perturbations across the shock front numerically, a single ω value used in the point run usually doesn't fill all of parameter space that makes up the totality of the evolution of the corrugation instability. This can be seen below in figure 3.3.

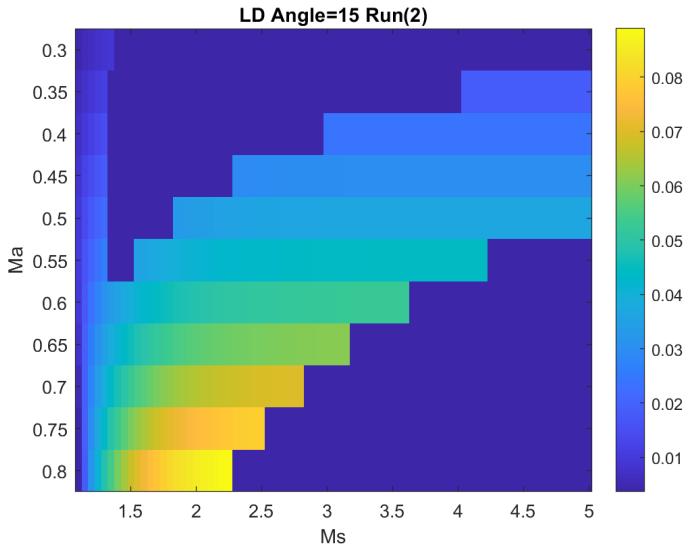

Figure 3.3: Low resolution model with a partial fill of parameter space for an Lessen and Deshpande (LD) case model at an angle input of $\beta = 15°$. Two ω values were used to the parameter space presented.

Figure 3.3 seeks to visualize the evolution of the corrugation instability for a shock front that has a fluid entering the shock front at angle of $\beta = 15$ with respect to the normal of the shock front. The dark blue region represents the parts of parameter space that require a different ω value solution that solves the stitched ideal MHD equations. This dark blue region indicates the trivial ω value solution of zero which can be improved upon by choosing that piece of parameter space and finding an ω value that fills that space. Running a second area search with the new coordinates of the part parameter space that needs to be filled produces a new ω value that is non trivial. Once a new ω value is found, the run type can be switched back to a point search run and the new ω value can be inputted. Running parallelcaseBatchLinogen again will produce a new plot with more of parameter space filled. This solution can be stitched together with the solution from the first point search run to ultimately create a plot that fills more of parameter space. This process is usually conducted more than once to produce sufficient plots that model the corrugation instability across

all of parameter space.

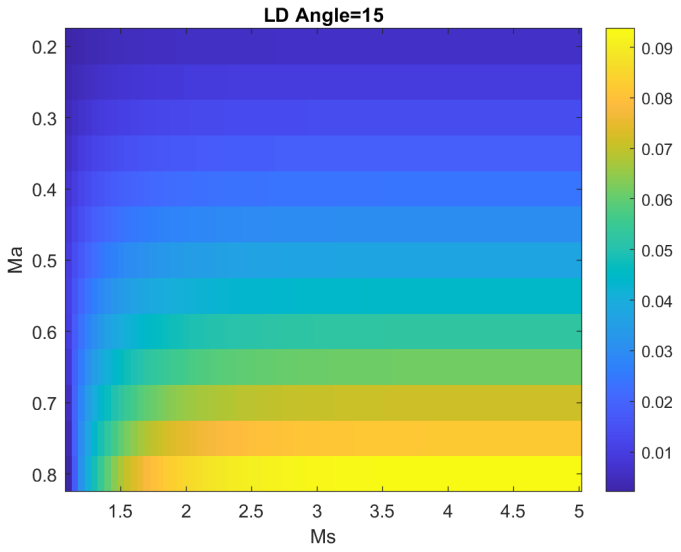

Figure 3.4: Low resolution model with all of parameter space filled for an Lessen and Deshpande case model at an angle input of $\beta = 15°$. Nine ω values were found and used to fill all of parameter space.

Once all of parameter space is filled in the low resolution model as shown in figure 3.4, the step conditions for the model can be increased to produce a higher resolution model. To create the high resolution model, the original data from the low resolution model that is stored in MATLAB's data manager will need to be cleared. Since the ω values have already been found that fill all of parameter space, no area searches need to be done and the ω values can be inputted and the can be code run. After running each ω value in the point search run, the solution will need to be stitched together with the previous ω value solution similar to what was done with the low resolution model. This process must repeated for every ω value that is newly inputted to fill all of parameter space.

Chapter 4

Results

4.1 Shock Evolution

The evolution of the shock front is modeled over the Alfven Mach number (Ma) and the sonic Mach number (Ms). Two separate cases were studied to further understand the corrugation instability of slow shocks. The first case is the Lessen Deshpande Case (LD Case). This case considers the input parameter Kz to be zero. Kz is the transverse z-component of the wave vector, $\vec{k}$, that activates Alfven waves that propagate away from the shock front both upstream and downstream. The second case studied is the general case. The general case accounts for the transverse z-component, Kz, to be nonzero. This research seeks to the visualize the differences in the evolution of the corrugation instability affected by the transverse z-component of the wave vector and the entry angle of the simulated fluid.

4.1.1 Lessen and Deshpande Case

In studying the Lessen and Deshpande (LD) Case, fluid entry angles were ranged from $\beta = 15°$ to $\beta = 45°$. In total, six high resolution models were created that describe the unstable growth of the perturbations to the shape of the shock front. In each model, a color bar was fixed to the right of the model to be used as a guide in understanding what the colors in each model indicate. Dark blue regions represent areas of little to no growth to the perturbations to the shape of the shock front. The shock front in stable in these regions. The yellow regions indicate that the shock undergoes maximum growth to the perturbations alternating the shock front's shape. The color bar's scale change based on the overall size of growth rate of the corrugation instability.

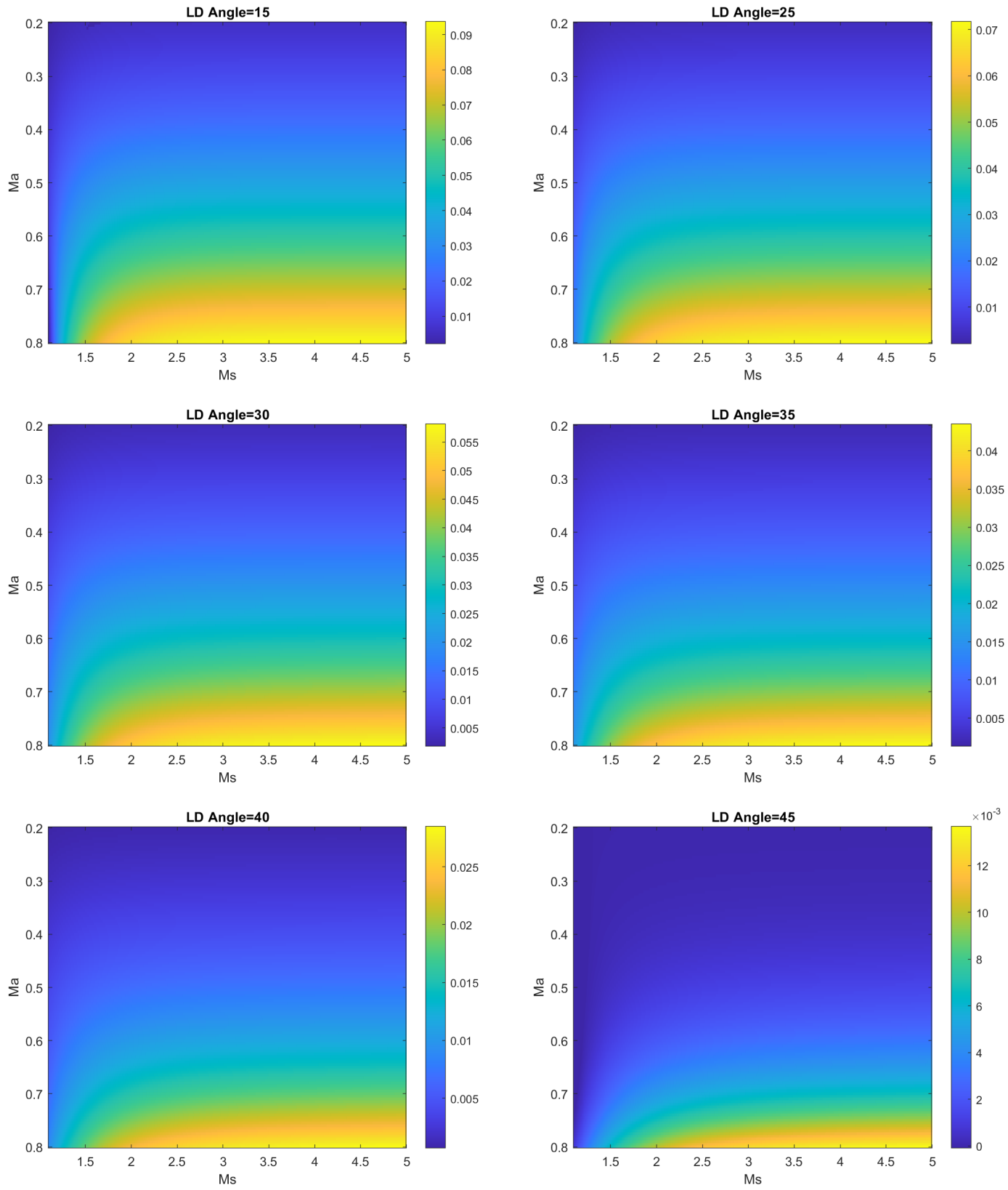

Figure 4.1: Lessen and Deshpande models for $\beta = 15°$ to $\beta = 45°$ and Kz=0.

Looking further at figure 4.1, it can be seen that the growth rate of the corrugation instability decreases as the entry angle, β, increases. Comparing $\beta = 15°$ to $\beta = 30°$, the yellow region is seen to begin at lower Mach numbers of Ms and Ma for $\beta = 15°$. This indicates that fluids moving at lower Mach numbers at $\beta = 15°$ cause the corrugation instability to grow more unstable than for fluids with $\beta = 30°$. This can futher be seen with $\beta = 45^{circ}$. At this fluid entry angle, the unstable growth region is a fraction of the size of the unstable growth region for a fluid at entry angle $\beta = 15°$ or even at $\beta = 30^{circ}$. At $\beta = 45^{circ}$ it can also be seen that for Ms ranging from [1.5,5] and Ma=0.4, there is a dark blue region that indicates that there is no growth to the perturbation of the shape of the shock front. This indicates that in this region, the shock front is stable. This region primarily indicates that the at this entry angle, the fluid has a strong enough magnetic field to hinder the growth to the perturbations that change the shape of the shock front.

Considering equation 2.17, the Alfven Mach number is inversely proportional to the initial magnetic field of the fluid entering the shock front. Therefore, increasing the magnetic field strength results in lower Alfven Mach numbers. For all Lessen and Deshpande models, lower sonic and Alfven Mach numbers resulted in minimal to no growth of the corrugation instability. Looking at an Alfven Mach number of Ma=0.2 for all models, the dark blue region indicates that there is no growth to the corrugation instability. Edelman concluded that slow shocks are unstable in the presence of low magnetic field strength and that the growth rates of the perturbations made to the shape of the shock rapidly decreases with an increase in the strength of the magnetic field [3]. Therefore, slow shocks are stable in strong magnetic fields.

The angle of the entry fluid affected the range of Alfven Mach numbers at which there was no growth of the corrugation instability for each model. Comparing $\beta = 15°$ to $\beta = 45°$, $\beta = 15°$ had a smaller stability region than $\beta = 45°$. Between Ma=0.2 to Ma=0.5, $\beta = 15°$ had no growth of the corrugation instability indicated by the dark blue region where as between Ma=0.2 to Ma=0.7, $\beta = 45°$ had no growth of the corrugation stability. Therefore, increasing the fluid entry angle resulted in an increase in the range of Alfven Mach numbers where there was no growth to the wrinkling of the shock front.

4.1.2 General Case

In studying the General Case, fluid entry was considered for a series of four angles: $\beta = 15°$, $\beta = 25°$, $\beta = 35°$, $\beta = 45°$. The range of values for the transverse component Kz differed between the four models based on the ω values found for each model. Adding the z-component of the wave vector, $\vec{k}$, activates Alfven waves which propagate both upstream and downstream away from the shock front. These Alfven waves are not present when there is no z-component of the wave vector as studied in the Lessen and Deshande case.

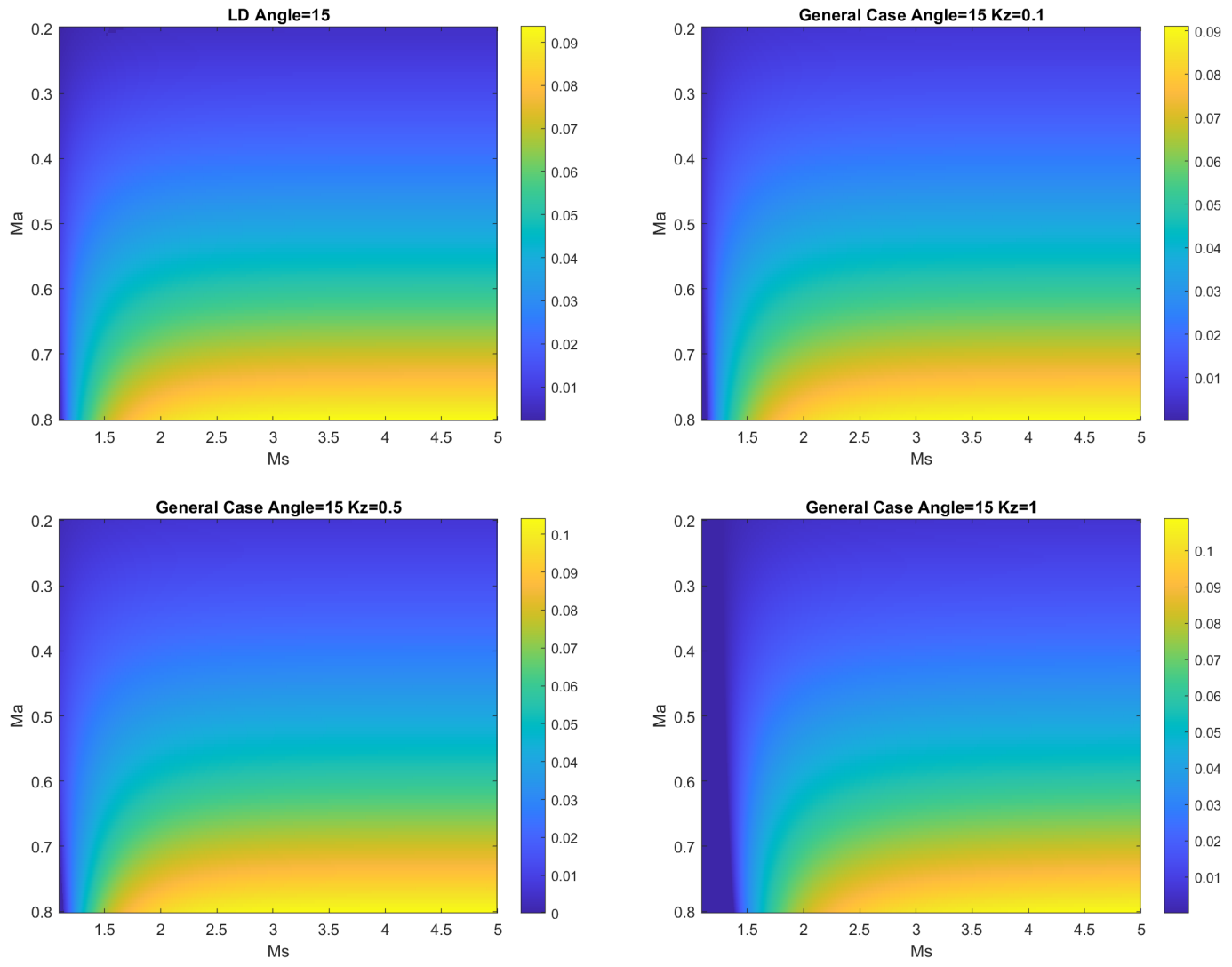

Figure 4.2: General case models for $\beta = 15°$ and Kz=0 to Kz=1

Comparing Kz=0 to Kz=1 for $\beta = 15°$, it can be seen that the plots begin "shifting" to the right. With this shift, a dark blue region arises for Ms=1.1 to Ms=1.5 ranging along the Ma values when Kz¿0. This indicates that there is no growth of the corrugation instability in that region of parameter space. There seems to be a growth in this pocket of parameter space ranging from Kz=0 to Kz=1. The anomaly arises with Kz=0.5. Given the trend of the growth of this pocket of parameter space, it would be expected that Kz=0.5 has more of this stable region of parameter space than kz=0.1 has. However, it does not. It can be seen however that Kz=0.1 has more growth of the corrugation instability. Adding a transverse z-component of $\vec{k}$ to the shock did not alter the shape of the growth of corrugation instability but shifted the sonic Mach number that activates growth in the corrugation instability. When Kz=0, growth of the corrugation instability could be seen at Ms=1.5 and Ma=0.8. When Kz=1, growth of corrugation instability could be seen at Ms=2 and Ma=0.8. Therefore it took a larger sonic Mach number to cause growth of the corrugation instability when Kz=1 than when Kz=0.

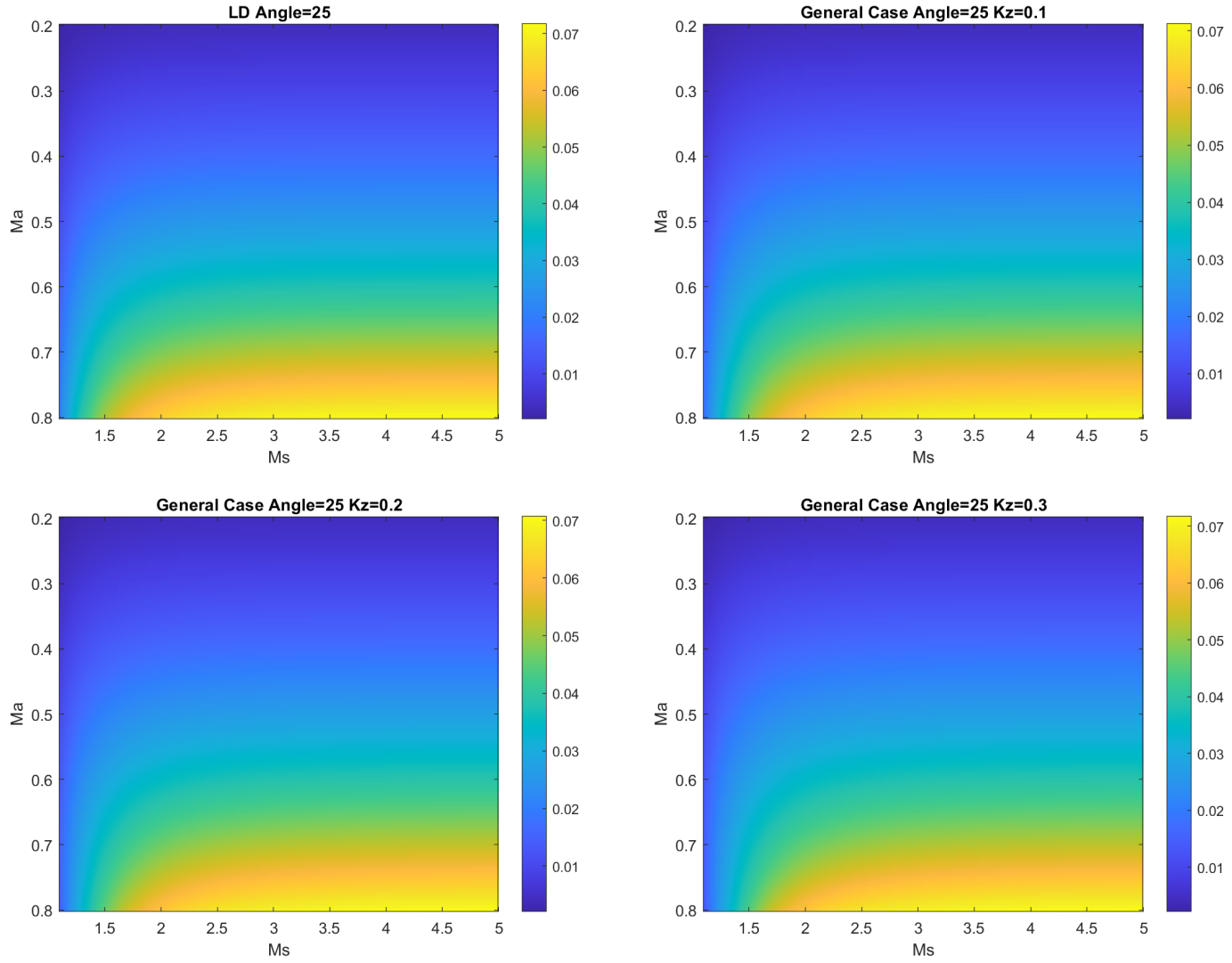

Figure 4.3: General case models for $\beta = 25°$ and Kz=0 to Kz=0.3

For $\beta = 25°$, models could only be created for Kz values up to 0.3. Past this Kz value, a few ω values reached a trivial solution where the real component of the ω value was equal to zero causing the creation of a plot that could model the growth of the corrugation instability to have empty regions of parameter space. Comparing Kz=0 to Kz=0.3 for $\beta = 25°$, the region where the most growth in the corrugation instability (the yellow region) was shifted along the sonic Mach number axis. For Kz=0, the increased growth in the corrugation instability began around Ma=0.8 and Ms=1.5. For Kz=0.3, the increased growth in the corrugation instability began around Ma=0.8 and Ms=1.6. Therefore, by increasing the value of Kz, the growth of corrugation instability began at higher sonic Mach numbers.

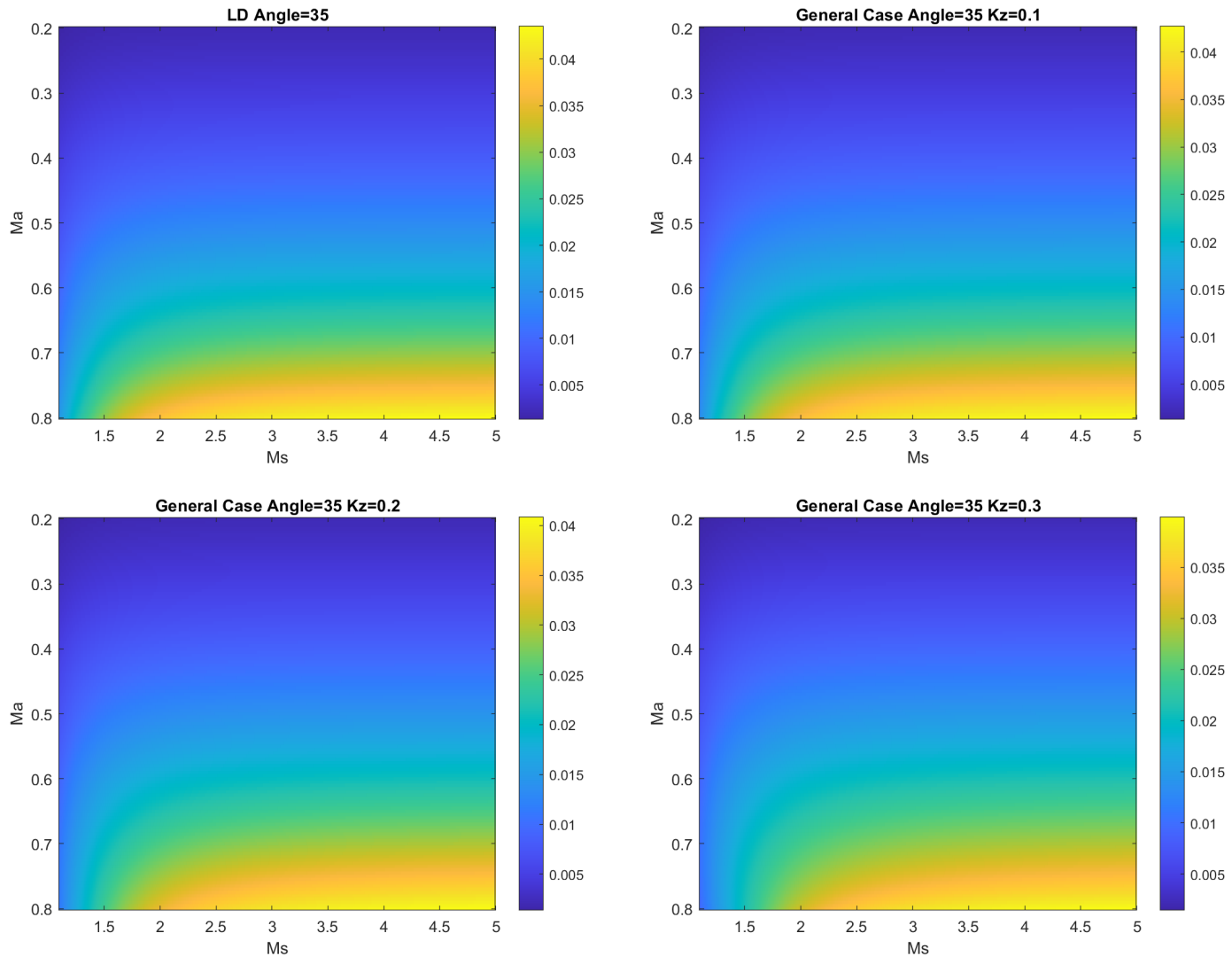

Figure 4.4: General case models for $\beta = 35°$ and Kz=0 to Kz=0.3

For $\beta = 35°$, models could only be created for Kz values up to 0.3. Past this Kz value, a few ω values reached a trivial solution where the real component of the ω value was zero causing the creation of a plot that could model the growth of the corrugation instability to have empty regions of parameter space similar to $\beta = 25^{circ}$. Comparing Kz=0 to Kz=0.3 for $\beta = 25°$, the region where the most growth of the corrugation instability occurred(the yellow region) was shifted along the sonic Mach number axis. For Kz=0, the increased growth of the corrugation instability began around Ma=0.8 and Ms=1.6. For Kz=0.3, the increased growth of the corrugation instability began around Ma=0.8 to Ms=2. Therefore, by increasing the value of Kz, the growth of corrugation instability began at higher sonic Mach numbers. This result is similar to that found for changing the Kz value of $\beta = 25°$. However, the shift of the growth of the corrugation instability along the sonic Mach number axis was greater for $\beta = 35°$ than for $\beta = 25°$.

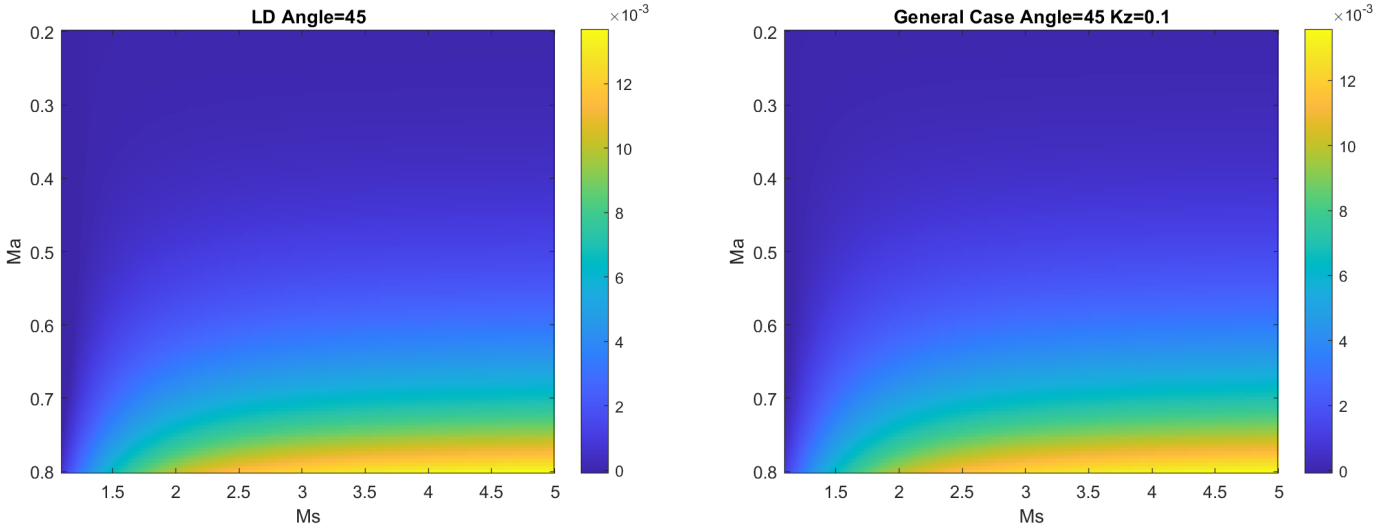

Figure 4.5: General case models for $\beta = 45°$ and Kz=0 to Kz=0.1

For $\beta = 45°$, models could only be made for Kz values ranging from Kz=0 to Kz=0.1. For Kz values past Kz=0.1, all ω values were trivial. Comparing Kz=0 to Kz=0.1, little to no change in the growth of the corrugation instability was discovered. Both models are nearly identical to each other.

Referencing equation 2.17, the Alfven Mach number is inversely proportional to the initial magnetic field of fluid entering the shock front. As discussed in the Lessen and Deshpande models, this proportionality indicates that stronger magnetic fields are present for lower Alfven Mach numbers. Changing the value of Kz did not change how the initial magnetic field of the fluid related to growth of the corrugation instability. That is, there was no vertical "shift" along the Alfven Mach number axis in all general case models when the value of Kz was increased. The only shift as a result of increasing Kz occurred horizontally along the sonic Mach number axis affecting the sonic number at which the growth of the corrugation instability began. Therefore, changing the value of Kz had no influence on the initial magnetic field of the entering fluid's role in affecting the growth of the corrugation instability.

Chapter 5

Conclusion

5.1 Corrugation Instability in Astrophysical Systems

The goal of this project is to examine how the growth of the corrugation instability in slow shock fronts change over a series of different fluid entry angles and transverse z-components of the wave vector, $\vec{k}$. This was achieved by modeling the growth of the corrugation instability in the Lessen and Deshande case where the transverse z-component of the wave vector was given a value equal to zero and the general case where the transverse z-component of the wave vector was given a nonzero value. Corrugation instability define the stability of a perturbed shock front over a series of Alfven and sonic Mach numbers. In the following plots, fluid speed increases with an increase in the sonic Mach number (Ms) and fluid magnetic field strength of the fluid decreases with an increase in the Alfven Mach number (Ma). The series of fluid entry angles modeled ranged from $\beta = 15°$ to $\beta = 45°$ with respect to the normal of the shock front for both studied cases. For the general case, the range of transverse z-components of the wave vector was unique to each fluid entry angle studied. The magnitude of the initial magnetic field of the fluid that passes through the shock front and its effect on corrugation instabilities was also analyzed over both cases.

Shown in figure 4.1 for the Lessen and Deshpande Case, as the angle increased, the range of sonic Mach numbers that the growth of the corrugation instability depended on became smaller. Higher sonic Mach numbers defined more growth in the corrugation instability in each model as the fluid entry angle increased. Across all angles, as the Alfven Mach number decreased, little growth in the corrugation stability was seen. Low Alfven Mach numbers correlate to larger magnitudes of an entry fluid's initial magnetic field. Therefore, larger magnitudes of an entry fluid's initial magnetic field resulted in minimal to no growth of the corrugation instability of a specific model therefore making the shock front stable. The general case found that the addition of the transverse z-component of the wave vector resulted in a change in the range of sonic Mach numbers for which growth of the corrugation instability occurred. Seen in figure 4.2, 4.3, and

4.4 there was a horizontal "shift" in the sonic Mach number that activated growth in the instability as the transverse component was increased. Therefore, Kz values great than 0.1 required larger sonic Mach numbers to activate growth of the corrugation instability. It was also found that changing the value of Kz had no influence on the initial magnetic field of the entering fluid's role in affecting the growth of the corrugation instability.

5.2 Future Work

Further work could analyze a larger range of angles for the Lessen and Deshpande Case and the general case. This would give a greater overview of how the shock front is affected by the entry angle of the entering fluid. A sample set of fluid entry angles to study would range from $\beta = 0°$ to $\beta = 15°$ and $\beta = 45°$ to $\beta = 90°$. A larger range of transverse z-components of the wave vector could also be studied in an effort to paint a clearer picture of the overall effect that the transverse z-component of the wave vector has on the growth of the corrugation instability in the general case. It would also be interesting to take each model and find a function that models the growth of the corrugation instability. Doing this would add another aspect of analysis to this project that would seek to compare how the functions change for each case given the different parameter changes. Given more time, these are the next steps that would be taken to further add to this research.

Chapter 6

Acknowledgements

I would like to thank Dr. Janet Tate for the support and resources she provided over the last three terms during the process of this thesis. I would like to thank Dr. Randall Milstein and Dr. Henri Jansen for being members of my defense committee and for all their support over the past four years. I would also like to thank Dr. Kathryn Hadley. Kathy has been a wonderful mentor for me over these past three years and has helped me further my love for astrophysics. Her patience with my learning and work has meant a great deal to me and I hope to continue to work with her in the near future.

Chapter 7

References

[1] C.S. Gardner and M.D. Kurskal, Phys. Fluids 7, 700 (1964).

[2] Fitzpatrick, Richard. "MHD Waves." MHD Waves, The University of Texas.

[3] J.M. Stone and M. Edelmen, 1995, ApJ 454, 182.

[4] J.F. McKenzie and K.O. Westphal, 1970, Phys. Fluids, 13, 630.

[5] Kokalj, Janez. Magnetohydrodynamic Waves in Plasma. University of Ljubljana Department of Physics.

[6] M. Edelman, 1990b, Astrophysics, 31, 758.

[7] M. Lessen and N.V. Deshpande, J. Plasma Phys. 1, 463 (1967).

[8] Murphy, Nick. MHD Shocks and Discontinuities. Harvard-Smithsonian Center for Astrophysics, 22 Feb. 2016.

[9] Nakariakov, Valery. Magnetohydrodyanmics (MHD). KHU.

[10] Rasinkangas, Reijo. "Magnetohydrodynamic Waves ." Spacewiki, University of Oulu, 11 Oct. 2008.